SMOS Near-Real-Time Soil Moisture processor: Recommended neural network configuration and algorithm description

Nemesio Rodriguez-fernandez, Philippe Richaume, Joaquin Munoz-Sabater, Patricia de Rosnay, Yann H. Kerr

SMOS Near-Real-Time Soil Moisture processor:
Recommended neural network configuration and algorithm description

Release 1.6
23 March 2016

Prepared by

CESBIO

In cooperation with ECMWF

SMOS Near-Real-Time Soil Moisture processor.

Recommended neural network configuration and algorithm description.

ESA contract 4000101703/10/NL/FF/fk CCN4
Technical Officer: M. Drusch

CESBIO-SMOS report **SO-TN-CB-GS-0049 v1.6**

N.J. Rodríguez-Fernández[1], P. Richaume[1], J. Muñoz-Sabater[2], P. de Rosnay[2], Y.H. Kerr[1]

[1] **CESBIO**
UMR 5126 (CNRS, CNES, UPS, IRD),
18 av. Edouard Belin, bpi 2801, 31401 Toulouse cedex 9, France

[2] **ECMWF**
Shinfield Park, Reading, RG2 9AX, UK

March 23rd, 2016

This document is the Technical Report 1 (TR1) for Work Package 4020 and was compiled for the ESA-ECMWF contract 4000101703/10/NL/FF/fk CCN4.

Number of pages: 30

Authors:	N.J. Rodríguez-Fernández, P. Richaume, J. Muñoz-Sabater, P. de Rosnay, Y.H. Kerr		
Circulation:	ESA document.		
Release	Date	Details	Editor
1.1	16 Dec 2014	First draft	NRF
1.2	14 Jan 2015	Comments from PdR	NRF
1.3	20 Apr 2015	Analysis of best strategy to compute I_2 Including NN specifications Validation against ISMN data	NRF
1.4	15 Jul 2015	Including temporal correlation maps and monthly averages for the proposed NRT NN configuration	NRF
1.5	1 Dec 2015	Including error computation Updated flow chart	NRF NRF
1.6	23 Mar 2016	Comments by ESA (MD)	NRF

For any clarifications please contact N. Rodríguez-Fernández or Y. Kerr (nemesio.rodriguez@cesbio.cnes.fr, yann.kerr@cesbio.cnes.fr).

Project partners

Contractor	**ECMWF**, Reading (United Kingdom)
Co-Contractor	**CESBIO**, Centre d'Etudes Spatiales de la BIOsphère, Toulouse, (France).

Contents

List of Figures

List of Tables

Reference documents

Technical report 2	Muñoz-Sabater et al. (2016)

1 Executive summary

The best approach to retrieve soil moisture in Near-Real-Time (NRT) using neural networks (NNs) has been discussed using SMOS CATDS Level 3 brightness temperatures and Level 3 soil moisture (SM). NN retrievals have been first evaluated comparing the output SM to the L3 SM. The NN output has also been evaluated against in situ measurements over the SCAN network, the USDA ARS watersheds and OzNet. The recommended input configuration for the NRT SM processor is using SMOS T_{b}'s from 30° to 45 ° incidence angles in 5° bins for both H and V polarizations, and a corresponding set of normalized indexes computed taking into account the brightness temperatures local extreme values and the associated L3 SM values. Finally, the input data should add the 0-7 cm soil temperature forecast by ECMWF. The recommended NN architecture is two layers with a hidden layer containing 5 non-linear neurons and an output layer with one linear neuron. This configuration is the best trade-off of retrieval performance and swath width (914 km). The recommended NN configuration for the NRT SM product has been specifically evaluated against the reference L3 SM data and against a large number of in situ measurements from the International Soil Moisture Network. Average statistics are somewhat better than those of the reference L3 SM data for most of the sites. In summary, the recommended NN configuration performs as well or better than the reference SM dataset but the retrieval can be done in NRT after a global training phase.

In addition to the description of the best NN configuration to retrieve SM in NRT, the algorithm theoretical basis are discussed in detail, including the output uncertainty estimation. Finally, the architecture of the operational implementation is described. The actual NRT SM processor implementation and the final product evaluation can be found in Muñoz-Sabater et al. (2016).

2 Introduction

The objective of this document is to study the best neural network (NN) configuration to implement a Near-Real-Time (NRT) soil moisture (SM) processor from SMOS observations. The recommended NN configuration for the NRT operational processor is described and the algorithm theoretical basis are discussed in detail. Finally, the architecture of the operational implementation is also described. The actual NRT SM processor implementation and the final product evaluation can be found in Muñoz-Sabater et al. (2016). Further evaluation of the NRT SM product globally with respect to the operational SMOS Level 2 SM and locally with respect to *in situ* measurements in North America can be found in Muñoz-Sabater et al. (2016).

This work follows that of the ESA SMOS+"Neural Network" (SMOS+NN) project (Rodríguez-Fernández et al., 2013, 2014, 2015), whose objectives were to do a feasibility study of the use of neural networks to retrieve SM from SMOS observations.

The NRT SM product should be as similar as possible to the operational L2 SM product and it should be provided in the same grid (ISEA grid common to L1 and L2 ESA products). A NRT processor needs to find a trade-off in between the best retrieval quality and the larger swath-width. Therefore, the work done during the SMOS+NN project has been extended using different combinations of incidence angle ranges from 1 (40-45 deg) to 7. The exact angle range for each

model configuration and the associated swath half-width is given in Table 1. Using SMOS brightness temperatures ($T_{\rm b}$'s) only in the 40°-45° incidence range allows SM retrievals in the full swath (2×588 km). Increasing the number of angle bins decreases the width of the swath where SM can be retrieved. For instance, the swath width will be 2×457 km or 2×334 km when using angles in the 30-45° or in the 25-60° range, respectively. Figure 1 shows a comparison of those three swath widths over Africa and Western Europe.

The SMOS+NN (Rodríguez-Fernández et al., 2013) database has been used to train NNs using SMOS $T_{\rm b}$'s, MODIS NDVI, ECMWF soil temperature and ECOCLIMAP soil texture as input. Taking into account the constrains of a NRT SM product (Sect. 2), the SMOS L3 SM has been used as reference for the supervised learning phase. Both Level 3 SM and $T_{\rm b}$'s are CATDS data version RE01.

The training and evaluation strategy of Rodríguez-Fernández et al. (2013) has been adopted. The NN has been trained using data from November 2010 to December 2012, taking one day every five and one grid point over three both in longitude and latitude. This database contains 5 millions vectors. The total number of vectors available for the training depends on the number of angle bins required as input for the NN. For instance, requiring a well defined value of the $T_{\rm b}$ for both polarizations and three angle bins from 30° to 45°, there are $7.9\,10^5$ vectors, of which $5.5\,10^5$ have an associated L3 SM value and can be used for the "training" dataset (actually used for training, validation and tests). This training dataset, is divided in three disjoint subsets that are selected randomly. A subset of 60 $\%$ of the "training" dataset ($3.3\,10^5$ vectors in the previous example) is used for the actual training and determination of the NN weights. A subset of 20 $\%$ of the "training" dataset ($1.1\,10^5$ vectors in the previous example) is used as validation dataset to evaluate, iteration per iteration, the performance of the NN during the training phase and stop the training in there are signs of over-learning. No over-learning has been detected for any of the NNs. The final 20 $\%$ of the "training" dataset is used to evaluate *a posteriori* the correlation, RMSE and mean absolute error (MAE) of the NN output with respect to SMOS L3 SM. The results are listed in columns 2 to 4 of Table 2.

In addition, the NN results have been evaluated against *in situ* measurements of the USDA SCAN networks (Schaefer et al., 2007), the USDA watersheds networks in the USA (Jackson et al., 2012) and representative stations of the Australian OzNet network (Smith et al., 2012). The mean STD, R and bias of the output of each NN configuration with respect to the *in situ* measurements are listed in columns 5-7 of Table 2. For comparison purposes, the ECMWF IFS (Integrated Forecasting System) operational top layer (0-7cm) soil moisture and the SMOS L3 SM evaluation against in situ measurements is shown in Table 1.

Finally, for some of the NN configurations, the trained NN has been used to invert three years of SMOS data from 1/6/2010 to 23/6/2013 and the retrieved NN SM has been compared to SMOS L3 SM as follows (see also Rodríguez-Fernández et al., 2015). Using this three-dimensional dataset (latitude, longitude and time), two correlations of the NN SM and SMOS L3 SM datasets have been computed: *(i)* across the latitude/longitude plane (hereafter spatial correlation, R_{spa}) and, *(ii)* along the time axis (hereafter temporal correlation, R_{temp}). More specifically, R_{spa} is the Pearson correlation of SMOS L3 SM and NN SM for all the grid points observed a given day. Column 8

of Table 2 shows the mean of all daily values of R_{spa} from 1/6/2010 to 23/6/2013. The temporal correlation R_{temp} is the Pearson correlation of NN SM and SMOS L3 SM computed locally for each grid point using the 3-years time series. From the maps of R_{temp} it has been computed the mean value (column 9 of Table 2). Some maps are shown in Fig. 2.

The rest of this document is organized as follows: Section 3 discusses different NN configurations using SMOS L3 SM data as reference for the training and taking into account the constrains of a NRT system. Section 4 presents an evaluation of the performances of the proposed NN configuration for the NRT SM product against SMOS L3 SM and *in situ* measurements of SM. Finally, Section 5 discusses the proposed NRT SM processor architecture and flow chart as well as the specifications of the neural network itself .

Table 1: Evaluation of ECMWF surface SM and SMOS L3 SM against in situ measurements (for the same period as those in Table 2). The results are presented as a function of the incidence angle range measured by SMOS (second column), which determines the swath width (third column). Columns 4-6 show the mean standard deviation, correlation and bias of different SM products with respect to the *in situ* validation sites. Note that the quality of the operational SMOS L3 SM product increases significantly as the number of incidence angles accessible to SMOS increases.

	Angle range (deg)	Swath width (km)	Mean STD	Mean R	Mean Bias
ECMWF	...	...	0.049	0.59	0.056
SMOS L3	40-45	1176	0.063	0.46	-0.019
SMOS L3	35-45	1078	0.062	0.48	-0.016
SMOS L3	30-45	914	0.064	0.50	-0.026
SMOS L3	25-45	758	0.061	0.52	-0.022
SMOS L3	25-60	668	0.058	0.53	-0.023

3 Best configuration for a NRT SM processor

3.1 Input data

Table 2 gives the results for NNs that use different datasets as input including SMOS information for different incident angle bins, NDVI, soil temperature and texture. The SMOS observables are $T_{\rm b}$'s but in addition a local normalization of the $T_{\rm b}$'s (index I_1 of Rodríguez-Fernández et al., 2013) and a local normalization of the $T_{\rm b}$'s scaled to the minimum and maximum local SM values (index I_2 of Rodríguez-Fernández et al., 2013) have also been studied.

It is possible to pre-process SMOS $T_{\rm b}$'s to compute a local index (hereafter index I_1) by normalizing from 0 to 1 the brightness temperature for each polarization and incidence angle. First, the maximum (T_b^{max}) and minimum (T_b^{min}) of the $T_{\rm b}$'s in the time series for a given latitude (λ) and longitude (ϕ) grid point and for each polarization and incidence angle bin. The local normalized index can be computed as:

$$I_{2_{\lambda\phi}}(t) = SM_{\lambda\phi}^{T_b^{min}} + [SM_{\lambda\phi}^{T_b^{max}} - SM_{\lambda\phi}^{T_b^{min}}] I_{1_{\lambda\phi}}(t) \quad (1)$$

Table 2: Global evaluation in 2012 with respect to SMOS L3 SM (columns 2 to 4, correlation, RMSE and Mean Absolute Error), statistics with respect to *in situ* measurements (columns 5 to 7, STD, R and Bias are the standard deviation of the differences time series, the Pearson correlation coefficients and the bias (mean of NN SM minus de mean of *in situ* SM) averaged across all the *in situ* sites). Finally the spatial and temporal correlation of 3 years times series with respect to SMOS L3 SM are given in columns 8 and 9. Some of the input configuration includes MODIS NDVI ("VI"), sand and clay fractions ("tex") and soil temperature in the 0-7 cm layer from ECMWF IFS ("T").

input	R	RMSE	MAE	STD	R	Bias	Mean R_{spa}	Mean R_{temp}
Using only Tb's								
T_b(H,V,30°-45°),T	0.81	0.065	0.041	0.052	0.50	-0.028	0.77	0.70
T_b(H,V,30°-45°),tex,VI	0.78	0.068	0.044	0.046	0.54	-0.025		
T_b(H,V,30°-45°),T,VI	0.81	0.063	0.040	0.048	0.51	-0.027		
T_b(H,V,30°-45°),T,tex	0.82	0.063	0.039	0.052	0.50	-0.025	0.78	0.70
T_b(H,V,30°-45°),tex,VI,T	0.83	0.061	0.038	0.049	0.51	-0.026	0.81	0.76
T_b(H,V,25°-60°),VI,T	0.85	0.052	0.032	0.051	0.57	-0.031		
T_b(H,V,25°-60°),T,tex	0.86	0.051	0.031	0.050	0.56	-0.028	0.82	0.79
T_b(H,V,25°-60°),VI,T,tex	0.86	0.051	0.031	0.050	0.57	-0.026	0.82	0.78
Using local normalization of T_b's (I_1)								
I_1&T_b(H,V,30°-45°),T	0.81	0.064	0.041	0.054	0.52	-0.028	0.77	0.73
I_1&T_b(H,V,30°-45°),T,tex	0.83	0.061	0.039	0.054	0.51	-0.027	0.78	0.74
I_1&T_b(H,V,30°-45°),VI	0.78	0.068	0.045	0.051	0.54	-0.026		
I_1&T_b(H,V,30°-45°),VI,T	0.82	0.062	0.039	0.050	0.53	-0.030	0.79	0.77
I_1&T_b(H,V,30°-45°),VI,tex	0.79	0.067	0.044	0.050	0.56	-0.027		
I_1&T_b(H,V,30°-45°),VI,T,tex	0.83	0.061	0.038	0.051	0.53	-0.026		
I_1&T_b(H,V,25°-45°),T	0.83	0.060	0.037	0.054	0.53	-0.030		
I_1&T_b(H,V,25°-45°),VI	0.79	0.066	0.043	0.052	0.57	-0.029		
I_1&T_b(H,V,25°-45°),VI,T	0.83	0.059	0.037	0.052	0.55	-0.030		
I_1&T_b(H,V,25°-60°),T	0.85	0.051	0.032	0.050	0.56	-0.030	0.82	0.79
I_1&T_b(H,V,25°-60°),VI	0.81	0.058	0.037	0.049	0.58	-0.030		
I_1&T_b(H,V,25°-60°),VI,T	0.86	0.051	0.031	0.052	0.57	-0.029	0.82	0.79
Using local normalization of T_b's with SM extreme values (I_2)								
I_2&T_b(H,V,40°-45°)	0.83	0.060	0.039	0.045	0.51	-0.024		
I_2&T_b(H,V,40°-45°),T	0.85	0.056	0.036	0.043	0.49	-0.025	0.86	0.71
I_2&T_b(H,V,40°-45°),VI	0.85	0.057	0.037	0.038	0.54	-0.024		
I_2&T_b(H,V,40°-45°),VI,T	0.87	0.054	0.034	0.039	0.50	-0.024	0.87	0.74
I_2&T_b(H,V,35°-45°)	0.86	0.055	0.036	0.048	0.52	-0.021		
I_2&T_b(H,V,35°-45°),T	0.89	0.050	0.031	0.045	0.51	-0.022	0.87	0.72
I_2&T_b(H,V,35°-45°),VI	0.88	0.052	0.033	0.042	0.54	-0.022		
I_2&T_b(H,V,35°-45°),VI,T	0.89	0.048	0.030	0.042	0.52	-0.021	0.88	0.74
I_2&T_b(H,V,30°-45°)	0.89	0.048	0.032	0.051	0.54	-0.023		
I_2&T_b(H,V,30°-45°),T	**0.92**	**0.043**	**0.027**	**0.049**	**0.55**	**-0.024**	**0.89**	**0.79**
I_2&T_b(H,V,30°-45°),VI	0.90	0.047	0.030	0.046	0.56	-0.022		
I_2&T_b(H,V,30°-45°),VI,T	0.92	0.042	0.026	0.047	0.55	-0.022	0.91	0.79
I_2&T_b(H,V,25°-45°)	0.91	0.044	0.029	0.052	0.55	-0.027		
I_2&T_b(H,V,25°-45°),T	0.93	0.038	0.023	0.050	0.55	-0.028		
I_2&T_b(H,V,25°-45°),VI	0.92	0.042	0.027	0.047	0.58	-0.030		
I_2&T_b(H,V,25°-45°),VI,T	0.94	0.037	0.023	0.048	0.56	-0.029		
I_2&T_b(H,V,25°-60°),VI	0.93	0.037	0.024	0.047	0.56	-0.033		
I_2&T_b(H,V,25°-60°),T	0.95	0.033	0.021	0.046	0.54	-0.031		
I_2&T_b(H,V,25°-60°),VI,T	0.95	0.032	0.020	0.048	0.55	-0.033	0.92	0.83

Where

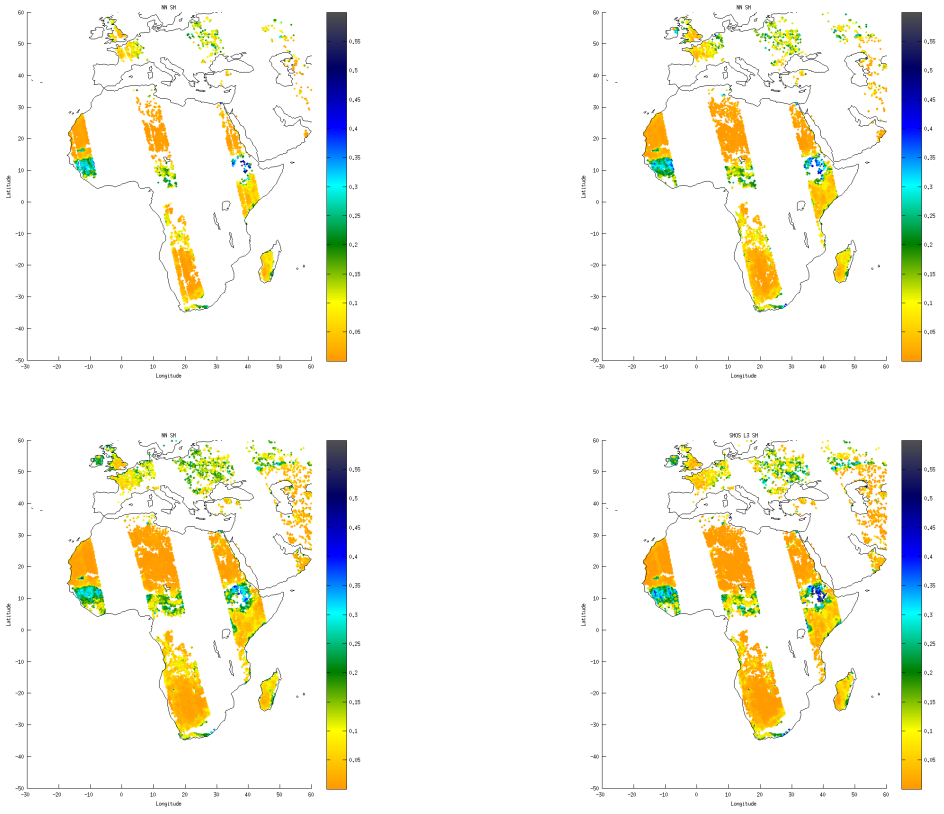

Figure 1: Soil moisture retrievals from NNs : [I_2&T_b/(H,V,25°-60°),VI,T] (upper left), [I_2&T_b(H,V,30°-45°),VI,T] (upper right) and [I_2&T_b(H,V, 40°-45°),VI,T] (bottom left) for day 1-8-2011. The bottom right is the SMOS L3 SM map for the same day. All the data correspond to SMOS ascending orbits.

$$I_{1_{\lambda\phi}}(t) = \frac{T_{m_{\lambda\phi}}(t)}{T_{D_{\lambda\phi}}} \tag{2}$$

With $T_{m_{\lambda\phi}}(t) = T_{b_{\lambda\phi}}(t) - T_{b_{\lambda\phi}}^{min}$ and $T_{D_{\lambda\phi}} = T_{b_{\lambda\phi}}^{max} - T_{b_{\lambda\phi}}^{min}$. As I_1, the index I_2 is computed for each incidence angle bin and polarization at the time t of the SMOS acquisition. The information content of index I_2 is very strong as it contains a local information on the dynamic ranges of both the measured T_b's and the model SM.

When using only T_b's as SMOS information, even adding additional input data, one should definitely use as many incidence angles as possible as all the quality metrics improve. In contrast, using index I_2, it is possible to obtain good results with less than 7 incidence angles and using less complementary data as input. *The best compromise is using three incidence angles as input (both for H and V polarizations) and soil temperature (NN [I_2&T_b(30°-45°), T]) as the quality metrics are within 3 % of those of NN retrievals using 7 incidence angles but the swath width is 250 km*

larger (up to 914 km). Using less incidence angles makes the quality metrics to decrease by 5-10 % and would require to use also NDVI as input to improve the results, which will introduce significant constrains in a NRT operational processor as MODIS data will also be needed.

It is interesting to note that *the performances of the NN retrieval [I_2&$T_{\rm b}$(30°-45°), T] with respect to in situ data (columns 5-7 of Table 2) are actually better than those of the operational SMOS L3 SM, and close to those of ECMWF SM_{0-7cm} (Table 1).*

Figure 2 show the maps of temporal correlation with SMOS L3 SM for different NN retrievals. The main differences arise in high northern latitudes, where R_{temp} increases for the NN retrievals that show a higher mean R_{temp} in Table 2.

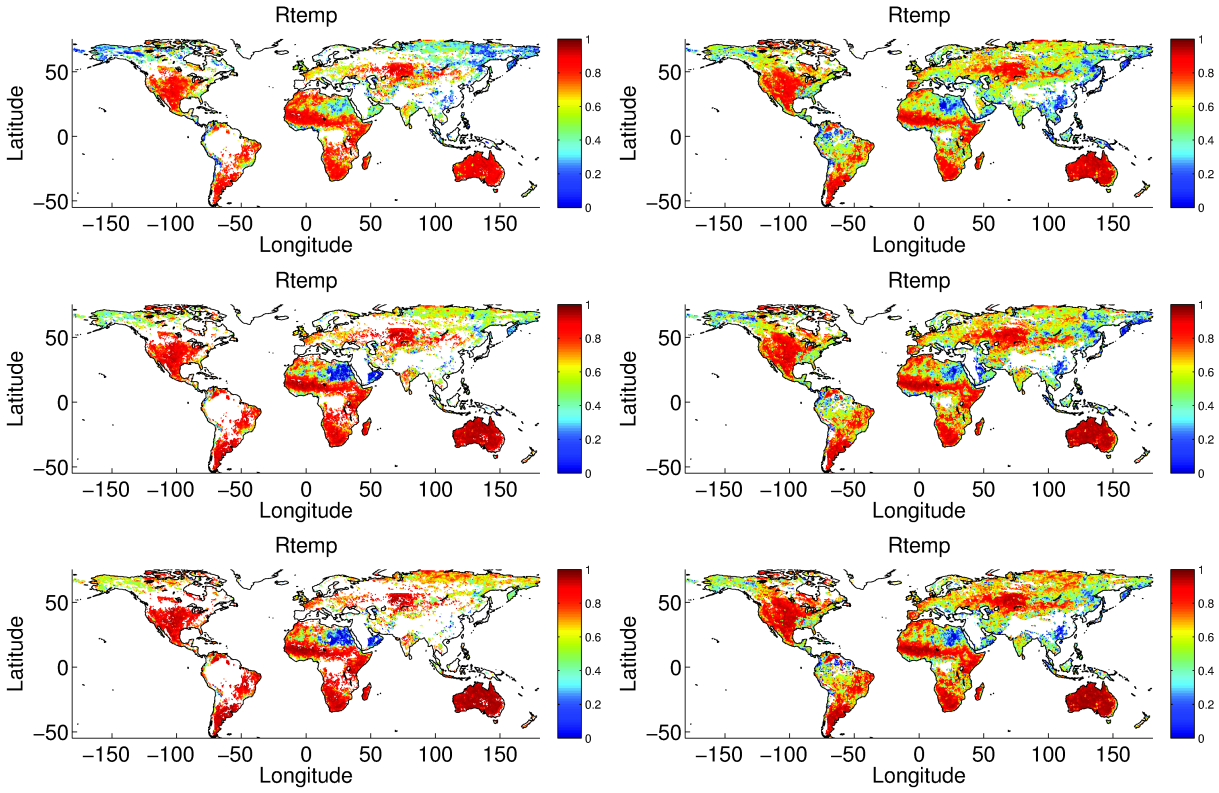

Figure 2: Temporal correlation for all grid points for NNs. Left panels, from top to bottom: [I_2&$T_{\rm b}$(H, V, 35°-45°), T, NDVI], [I_2&$T_{\rm b}$(H, V, 30°-45°), T, NDVI], [I_2&$T_{\rm b}$(H, V, 25°-60°), T, NDVI], Right panels, from top to bottom [I_1&$T_{\rm b}$(H, V, 30°-45°), T], [I_1&$T_{\rm b}$(H, V, 30°-45°), T, NDVI], [I_1&$T_{\rm b}$(H, V, 25°-60°), T].

3.2 Sensitivity to the probability of RFI

The R_{temp} values discussed in the previous sections have been computed after inversion of 3 years times series of NN SM for all grid points without taking into account the RFI probability as given in the SMOS SM product. It is pertinent to understand how a RFI probability threshold would change

the values presented in Table 2. Figure 3 and Table 3 show some maps and global statistics of the temporal correlation of NN SM and SMOS L3 SM for NN [I_1 & T_b's (H,V, 30°-45°), T, tex] and for different upper limits of the RFI probability. Some, but not all, of the globe regions with the lowest R_{temp} are actually regions with RFI probability higher than 10 %. Therefore, as expected the mean R_{temp} value over the globe increases as the RFI probability threshold decreases. Whether the NN SM is an improvement with respect to SMOS L3 SM in those regions of higher RFI probability and low R_{temp} would need further investigation. In any case, it is noteworthy that regions of low R_{temp} and low RFI probability still exist at northern latitudes.

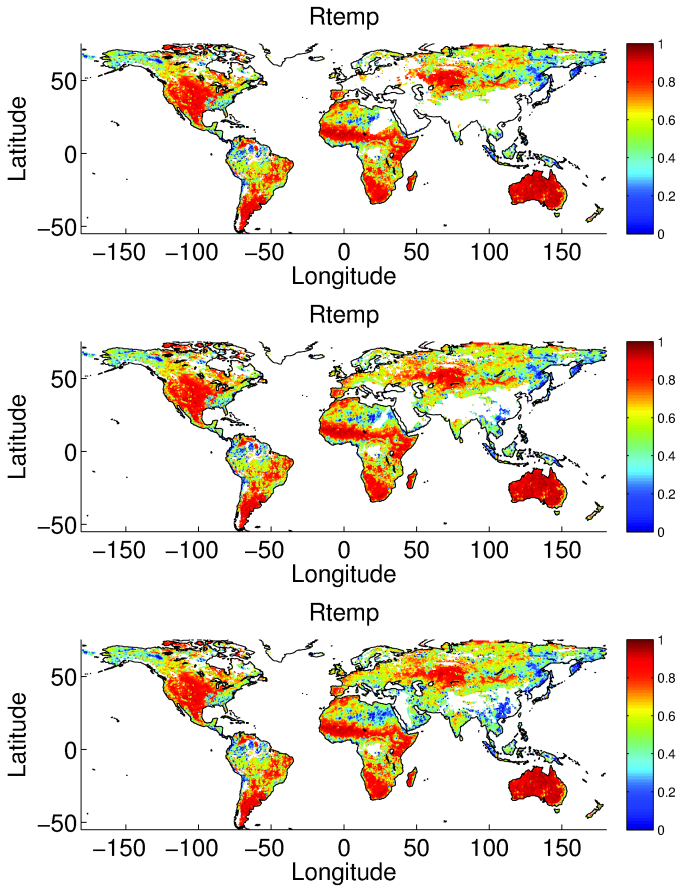

Figure 3: Temporal correlation for all grid points for NN [I_1&T_b(30°-45°), T, tex] and for an RFI probability lower than 10%, 20% or 100% (from top to bottom).

3.3 Computation of T_b's and SM local extremes tables

The effect of residual low level RFI in the computation of normalized indexes I_2 has been studied. RFI can affect significantly ${T_b}^{max}$ in some regions (Figure 4 shows an example in Northern Africa,

Table 3: Mean R_{temp} of the SM produced with NN[I_1&6T_b(30°-45°),T,tex] and SMOS L3 SM as a function of a RFI probability threshold

RFI Prob upper limit	Mean R_{temp}
100	0.74
20	0.76
15	0.77
10	0.78

Table 4: Performances of the non-linear regression (NN SM vs L3 SM) before and after requiring L3SM.

neurons	orbit	R	RMSE	MAE
without L3SM				
5	A	0.91	0.044	0.028
7	A	0.91	0.044	0.028
7	D	0.91	0.048	0.032
requiering L3SM				
5	A	0.89	0.046	0.029
7	A	0.90	0.045	0.028
7	D	0.90	0.048	0.031

Europe and the Middle Est). The upper-right panel of Figure 4 shows that it is possible to improve the computation of the ${T_b}^{max}$ values requiring a valid SMOS L3 retrieval for the point and the time of the ${T_b}^{max}$ acquisition.

In addition, requiring the existence of a valid SM value associated to the T_b guarantees the possibility of computing index I_2. Therefore more retrievals can be obtained (compare left and right middle panels of Figure 4).

An additional constrain to compute I_2 will be to compute T_b's percentiles and filter out the highest 10 % T_b's, for instance, to compute I_2. Nevertheless, it is worth noting that even if the input T_b's is unrealistic, using this T_b with the associated SM value computed with the operational algorithm will also be used by the NN as an additional constrain to invert the forward model.

Table 4 shows the NN SM performance with respect to L3 SM at global scale and Table 5 shows the evaluation against the same *in situ* sites used for Table 2. When a L3SM value is required to update the min/max tables the global performances of the NN SM both with respect to L3SM globally and with respect to *in situ* sites decrease slightly. The reason is that in this case one gets more retrievals using I_2, but actually those grid points are points with significant RFI probability, which make the global performances decrease.

3.4 Number of neurons

The effect of the number of neurons in the hidden layer has been evaluated by computing both the global performances with respect to L3 SM (Table 6) and with respect to *in situ* measurements

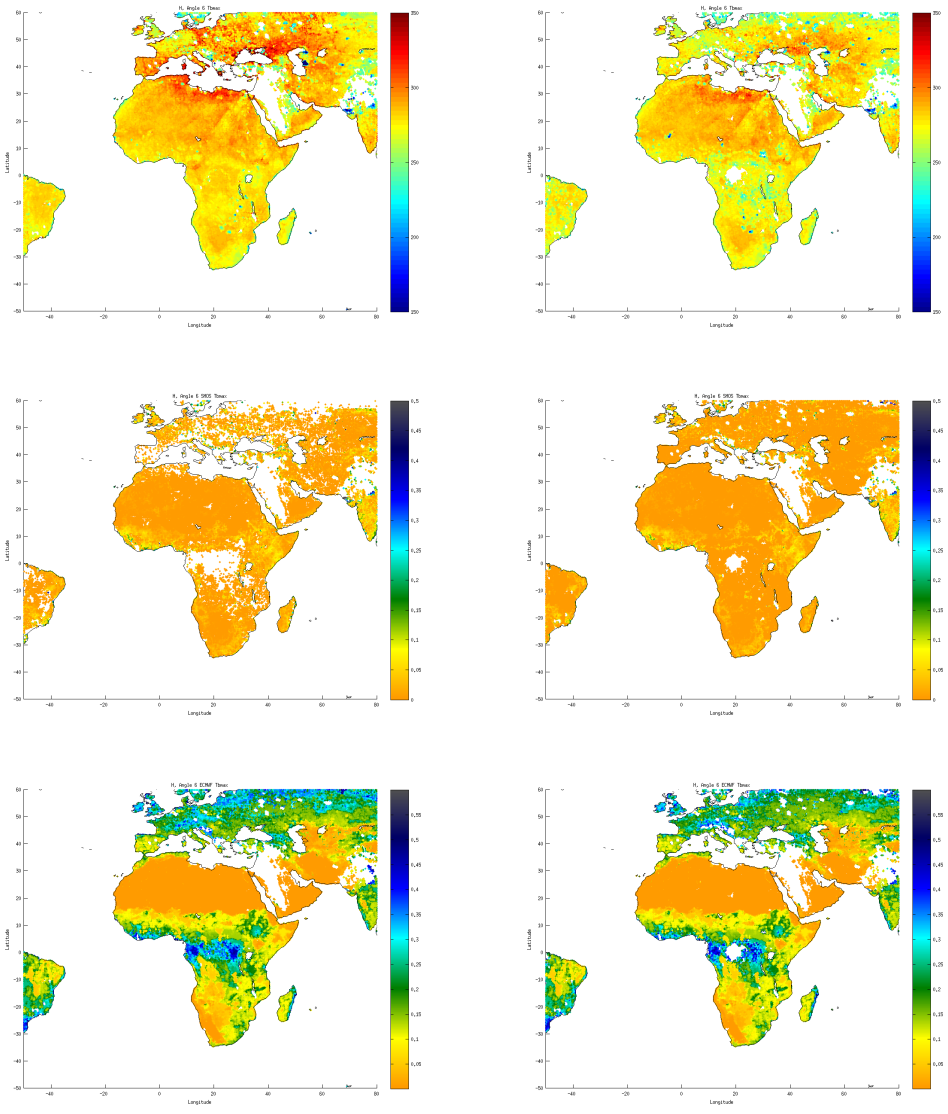

Figure 4: *Upper row,* $T_{\mathrm{b}}{}^{max}$*:* left no L3 SM constrain. Right: requiring an L3 SM retrieval to update the max-min table. Otherwise, a given high T_{b} is discarded. *Middle row, L3 SM associated to* $T_{\mathrm{b}}{}^{max}$*:* left no L3 SM constrain. Right: requiring an L3 SM retrieval to update the max-min table. Otherwise, a given high T_{b} is discarded. *Lower row, ECMWF layer 1 SM associated to* $T_{\mathrm{b}}{}^{max}$*:* left no L3 SM constrain. Right: requiring an L3 SM retrieval to update the max-min table. Otherwise, a given high T_{b} is discarded.

Table 5: Performances with respect to *in situ* measurements before and after requiring L3SM.

orbit	neurons	$< STD >$	R	$Bias$
without L3SM				
A	5	0.048	0.55	-0.022
A	7	0.049	0.54	-0.023
D	7	0.051	0.53	-0.035
requiring L3SM				
A	5	0.047	0.54	-0.028
A	7	0.048	0.54	-0.029
D	7	0.051	0.48	-0.032

Table 6: Performances of the non-linear regression (NN SM vs L3 SM) for different number of neurons in the hidden layer

neurons	orbit	R	RMSE	MAE
1	A	0.890	0.049	0.032
2	A	0.910	0.045	0.029
3	A	0.900	0.046	0.030
4	A	0.910	0.044	0.028
5	A	0.910	0.044	0.028
6	A	0.910	0.044	0.028
7	A	0.910	0.044	0.028
8	A	0.910	0.045	0.028
10	A	0.910	0.044	0.028
6	D	0.910	0.048	0.031
7	D	0.910	0.048	0.032
8	D	0.910	0.048	0.032

Table 7: Performances with respect to *in situ* measurements for different number of neurons in the hidden layer ("NN-nX" means NN with X neurons in the hidden layer). For comparison the statistics obtained by comparing ECMWF SM and SMOS L3 SM with respect to the *in situ* sites are also shown in the table.

orbit	SM	STD	R	$Bias$
A	NN-n1	0.047	0.53	-0.021
A	NN-n2	0.048	0.55	-0.023
A	NN-n3	0.047	0.55	-0.021
A	NN-n4	0.048	0.54	-0.022
A	NN-n5	0.048	0.55	-0.022
A	NN-n6	0.048	0.54	-0.023
A	NN-n7	0.049	0.54	-0.023
A	NN-n8	0.048	0.54	-0.023
A	NN-n10	0.048	0.54	-0.024
A	ECMWF	0.047	0.57	0.050
A	L3SM	0.062	0.51	-0.018
D	NN-n6	0.051	0.53	-0.036
D	NN-n7	0.051	0.53	-0.035
D	NN-n8	0.051	0.52	-0.035
D	ECMWF	0.056	0.58	0.056
D	L3 SM	0.065	0.48	-0.027

(Table 7).

The performances improve up to 4-5 neurons and remain constant for more neurons. *Therefore, for the shake of simplicity, the recommended architecture for the NRT processor is 5 neurons in the hidden layer* (and one neuron in the second or output layer).

4 Evaluation of the recommended NN configuration for the NRT SM processor

This section presents further evaluation of the SM dataset produced with the recommended configuration for the NRT SM processor, namely, using SMOS T_{b}'s from 30° to 45 ° incidence angles in 5° bins for both H and V polarizations, the corresponding I_2 normalized indexes, and the 0-7 cm soil temperature forecast by ECMWF. The NN architecture is two layers with a hidden layer containing 5 neurons.

A new training data base have been computed using one day every ten over the three years period and one grid point over three both in latitude and longitude. The maximum and minimum T_{b}'s tables (per incidence angle and polarization) have been updated only if a L3 SM value is available at the time of the T_{b} maximum.

4.1 Comparison to SMOS L3 SM

Figures 5 and 6 show the maps of temporal correlation of the NRT SM prototype with respect to the reference SMOS L3 SM both for ascending and descending orbits. The correlation of both products is very high (> 0.8) for all grid points except at high latitudes. The correlation at the Sahara desert is lower than the average, in particular for descending orbits. Lower correlation in this region of low SM values is expected because the relative error of SM is higher than in regions of higher SM values. Actually, Figure 5 also shows that the RMS of the difference of L3 SM with respect of NN SM is also very low in this region. In addition, the eastern Sahara can be affected by RFI souces in the Middle-East region. Further discussion can be found in Mecklenburg et al. (2016).

The NRT SM retrieval will be done orbit per orbit, however, to get further insight into the comparison of the NRT-prototype SM and L3 SM it is interesting to average the data over a larger period. Figure 7 shows a monthly average for July 2012 of SMOS L3 SM and the NRT SM. Both maps contains the same spatial structures. The difference map, also in Fig. 7, shows some underestimation of NRT SM with respect to L3 SM in regions of high SM values such as the tropical

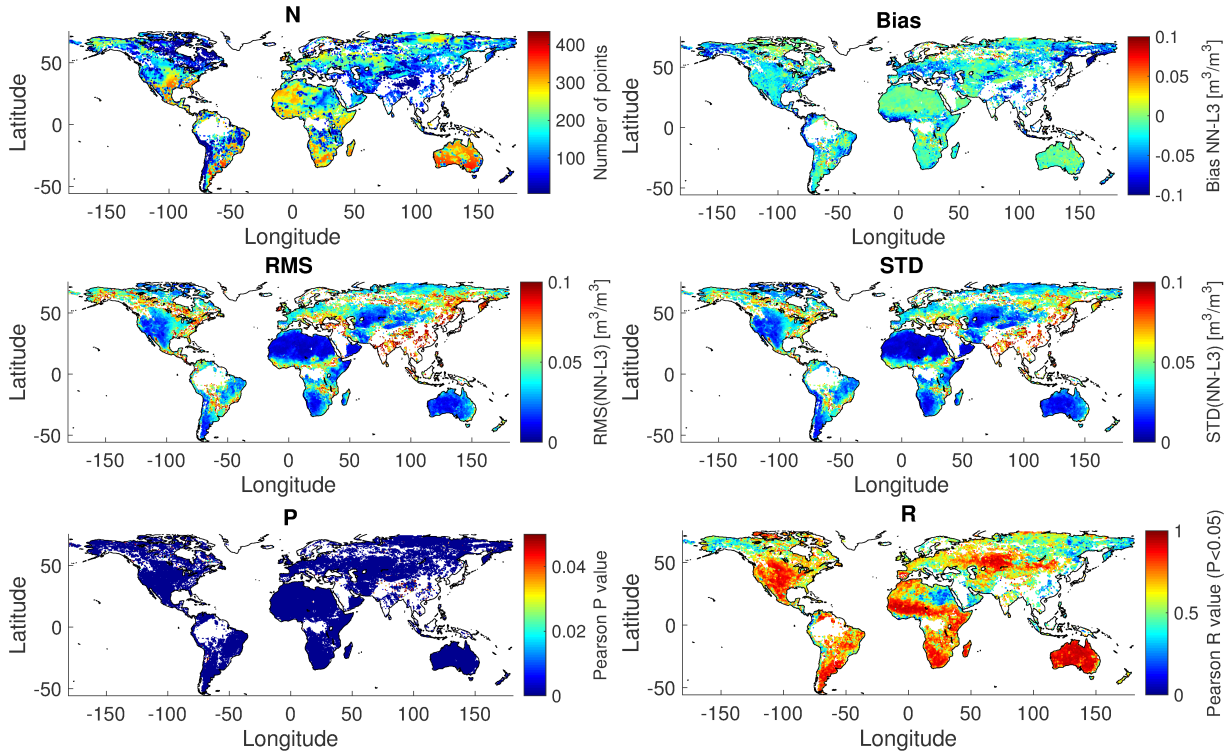

Figure 5: Comparison of SMOS L3 SM and the NN SM computed with the proposed configuration for the NRT product (angles from 30° to 45° plus soil temperature, one hidden layer with 5 neurons). N: number of points in the local time series. Bias: mean NN SM minus mean L3 SM. RMS: root mean square of the difference time series (NN SM - L3 SM). STD: standard deviation of the different time series. R: Pearson correlation coefficient. P: probability that the corresponding R value has been obtained by chance.

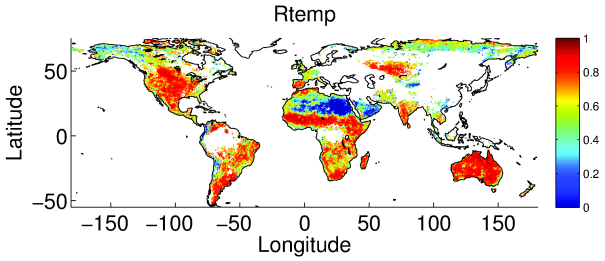

Figure 6: Same as the right-bottom panel of Fig. 5 but for descending orbits.

regions. The lower-right panel of Fig. 7 shows the standard deviation, the root-mean-squared error and the bias of the NRT SM with respect to L3 SM averaged in bins of SM. From 0 to 0.25 m^3/m^3 the average negative bias of NRT SM is lower than 0.02 m^3/m^3 while for the highest SM values (less well represented in the training data base) to negative bias can increase up to 0.04-0.05 m^3/m^3.

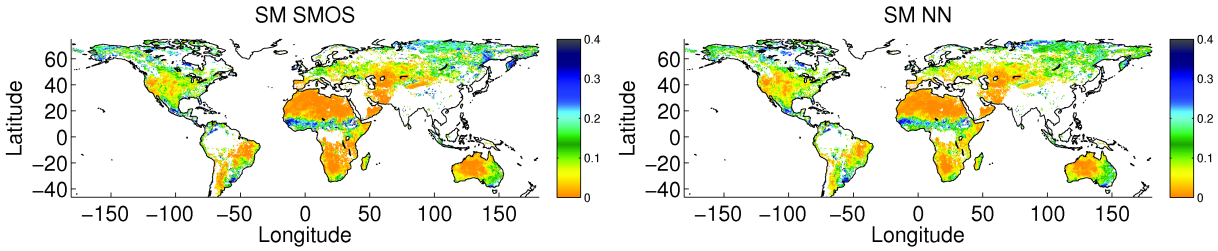

Figure 7: Comparison of the average SM computed for July 2012 using SMOS L3 SM (left) and NN SM (right) using the proposed configuration for the NRT product (angles from 30° to 45° plus soil temperature, one hidden layer with 5 neurons). Both maps correspond to ascending orbits.

4.2 Comparison to in situ measurements

The output of the proposed NRT NN configuration ($[6I_2, 6T_b, T]$ and 5 neurons in the hidden layer) has been further evaluated against a large number of *in situ* measurements retrieved from the International Soil Moisture Network (Dorigo et al., 2011). In addition, the SMOS L3 SM product and ECMWF IFS SM (0-7 cm) have also been evaluated against those measurements. For each in situ measurement, the closest CATDS grid point is selected. For this point the NRT SM, L3 SM and ECMWF SM are compared to the *in situ* measurement. The standard deviation, the Pearson correlation and the bias are computed using only times for which a SM value is available for the four datasets. Finally, the mean of those values over a given network of sensors is computed. Table 8 shows the results.

The values obtained for the NRT SM are comparable but somewhat better than those obtained with the L3 SM. For instance, the mean correlation with respect to in situ data is 15 % higher and the mean STD is lower by up to 0.02 m^3/m^3 than those of SMOS L3 for some networks such as

AMMA. The only two networks where SMOS L3 SM give slightly higher correlation with in situ data are OzNet for the 0-5 cm depth sensors and HOBE.

More detailed evaluation against *in situ* measurements analyzed as a function of vegetation parameters, topography or roughness can be found in Kerr et al. (2016).

Table 8: Evaluation of the proposed NN, ECMWF IFS (0-7 cm) and SMOS L3 SM against *in situ* measurements. NRT SM has been obtained using (6I2,6Tbs,T) as input and 5 neurons in the hidden layer. For each network, the table give the STD, Pearson R and Bias averaged across all the network sites taken into account (number of sites is given as "Sensors" and the average number of points in the time series is given as N_p). The upper and lower depth of the sensors is given in meters, following the network name.

SM	STD	R	$Bias$	STD	R	$Bias$
AMMA 0.05 0.05 : Sensors: 6; $N_p = 53$				SMOSMANIA 0.05 0.05 : Sensors: 13; $< N_p >= 62$		
NRT	0.061	0.566	0.009	0.047	0.613	-0.132
ECMWF	0.027	0.601	0.044	0.074	0.792	0.085
SMOS L3	0.069	0.476	0.003	0.069	0.611	-0.107
ARM .025 0.025 : Sites 9; $N_p = 124$				SCAN 0.05 0.05 : Sensors: 106; $N_p = 100$		
NRT	0.064	0.750	-0.062	0.048	0.533	-0.030
ECMWF	0.074	0.715	0.078	0.059	0.525	0.058
SMOS L3	0.084	0.679	-0.045	0.063	0.504	-0.023
RM 0.05 0.05 : Sensors: 16; $N_p = 128$				SNOTEL 0.05 0.05 : Sensors: 173; $N_p = 82$		
NRT	0.068	0.676	-0.158	0.041	0.454	-0.065
ECMWF	0.074	0.615	-0.051	0.045	0.471	0.040
SMOS L3	0.082	0.603	-0.143	0.058	0.391	-0.054
HOBE 0.00 0.05 : Sensors: 42; $N_p = 58$				UDC-SMOS 0.00 0.10 : Sensors: 1; $N_p = 34$		
NRT	0.053	0.470	-0.083	0.045	0.336	-0.266
ECMWF	0.044	0.617	0.026	0.025	0.529	-0.051
SMOS L3	0.075	0.500	-0.107	0.077	0.275	-0.196
OZNET 0.00 0.05 : Sites 8; $N_p = 36$				UDC-SMOS 0.05 0.05 : Sensors: 4 $N_p = 32$		
NRT	0.080	0.734	-0.022	0.046	0.301	-0.241
ECMWF	0.054	0.638	0.073	0.025	0.289	-0.027
SMOS L3	0.082	0.756	-0.051	0.078	0.297	-0.171
OZNET 0.00 0.08 : Sensors: 6; $N_p = 43$				USCRN 0.05 0.05 : Sensors: 53; N_p =115		
NRT	0.074	0.706	-0.016	0.053	0.603	-0.032
ECMWF	0.061	0.595	0.107	0.057	0.629	0.060
SMOS L3	0.082	0.611	0.001	0.066	0.549	-0.026
PBO-H2O 0.00 0.05 : Sensors: 6; $N_p = 111$				REMEDHUS 0.00 0.05 : Sensors: 4 $N_p = 173$		
NRT	0.048	0.718	-0.063	0.052	0.696	0.014
ECMWF	0.049	0.615	0.057	0.098	0.665	0.173
SMOS L3	0.059	0.616	-0.057	0.063	0.682	0.026

5 The NRT SM processor implementation

5.1 Global architecture

The structure of the NRT SM processor is shown in the flow chart depicted in Figure 8. The processor can be divided in three preprocessing blocks and the actual NRT SM processor containing the implementation of the NN.

ECMWF processor The first preprocessing block will extract information from ECMWF IFS such as snow depth soil temperature to filter out frozen soil or soil covered by snow. The soil temperature will also be used as input to the NN.

SMOS T_{b}'s processor The second preprocessing block is devoted to transform the NRT ECMWF SMOS T_{b}'s into a dataset similar to CATDS L3TB T_{b}'s (Berthon et al., 2013). The main steps consist in transform T_{b}'s in the antenna-based XY reference frame to the ground-based HV reference frame. A temporal interpolation of XY acquisitions should be done before to apply the rotation matrix to compute HV T_{b}'s as described by Quesney (2011). The second step will be to average the HV T_{b}'s in 5° incidence angle bins. Those operations should be applied to the NRT T_{b}'s that are distributed in BUFR format de Rosnay et al. (2012).

The off-line processor The third block is the off-line processor (grey box in Fig. 8), which is devoted to analyse the available time series of SMOS L2 SM to compute the SM values associated to the maximum and minimum T_{b}'s values for each polarization, incidence angle, and point of the ISEA grid. This is used to compute a maximum-minimum map that will be used to derive the local indexes I_1 and I_2. In the context of the on-line NRT SM processor it will only be needed to update the maximum-minimum table if new extreme values are measured.

In addition, the off-line processor to construct a training and a test database containing all the input information needed by the NN and SMOS L2 SM. An off-line pre-processing of two years of SMOS data will be needed to train and test the NN and compute weights and normalization parameters **described in Eqs. 3 to 6.**

Finally, the off-line processor has also been used to compute angle-binned T_{b} profiles in HV polarization from L1C data, in order to validate the output of the NRT T_{b}'s pre-processor.

NN NRT SM processor The core of the NRT SM processor is the NN processor, that will use the NN parameters to compute SM from the dataset prepared by the pre-processors. The output will be in the ISEA grid in NetCDF format. The output data will be

- The ISEA grid point number
- Latitude
- Longitude

Table 9: Input vector elements. The numbers in parenthesis in the second column is the center of the incidence angle bin in degrees.

	Elem.
$i = 1$	$I_2^H(32.5)$
2	$I_2^H(37.5)$
3	$I_2^H(42.5)$
4	$I_2^V(32.5)$
5	$I_2^V(37.5)$
6	$I_2^V(42.5)$
7	$T_b^H(32.5)$
8	$T_b^H(37.5)$
9	$T_b^H(42.5)$
10	$T_b^V(32.5)$
11	$T_b^V(37.5)$
12	$T_b^V(42.5)$
$n_{in} = 13$	$T_{(0-7cm)}$

- Year
- Month
- Day
- Seconds from midnight (all times should be UT)
- NRT soil moisture
- Soil moisture uncertainty
- RFI probability

Name conventions : file name conventions should follow ESA guidelines similar to those of the currently operational L2 SM product.

5.2 NRT SM algorithm

The NN used in the previous section has two layers. The first layer contains $j = 1, ..., n_{L1}$ nodes or neurons with an hyperbolic tangent as activation function. The second layer contains a single neuron with a linear function as activation function.

The number of elements in the input vector depends on the NN retrieval as discussed in Sect. 3. In the case of the recommended NN retrieval, using 6 $T_{\rm b}$'s (H and V for incidence angle bins from 30 to 45°), 6 index I_2 (H and V for incidence angle bins from 30 to 45°), and ECMWF soil Temperature, the number of elements n_{in} is 13. The order of the $i = 1, ..., n_{in}$ elements in the input vector should be preserved as the trained NN should be applied to an input vector v of the same characteristics than those used for the training. The recommended order of the elements is given in Table 9.

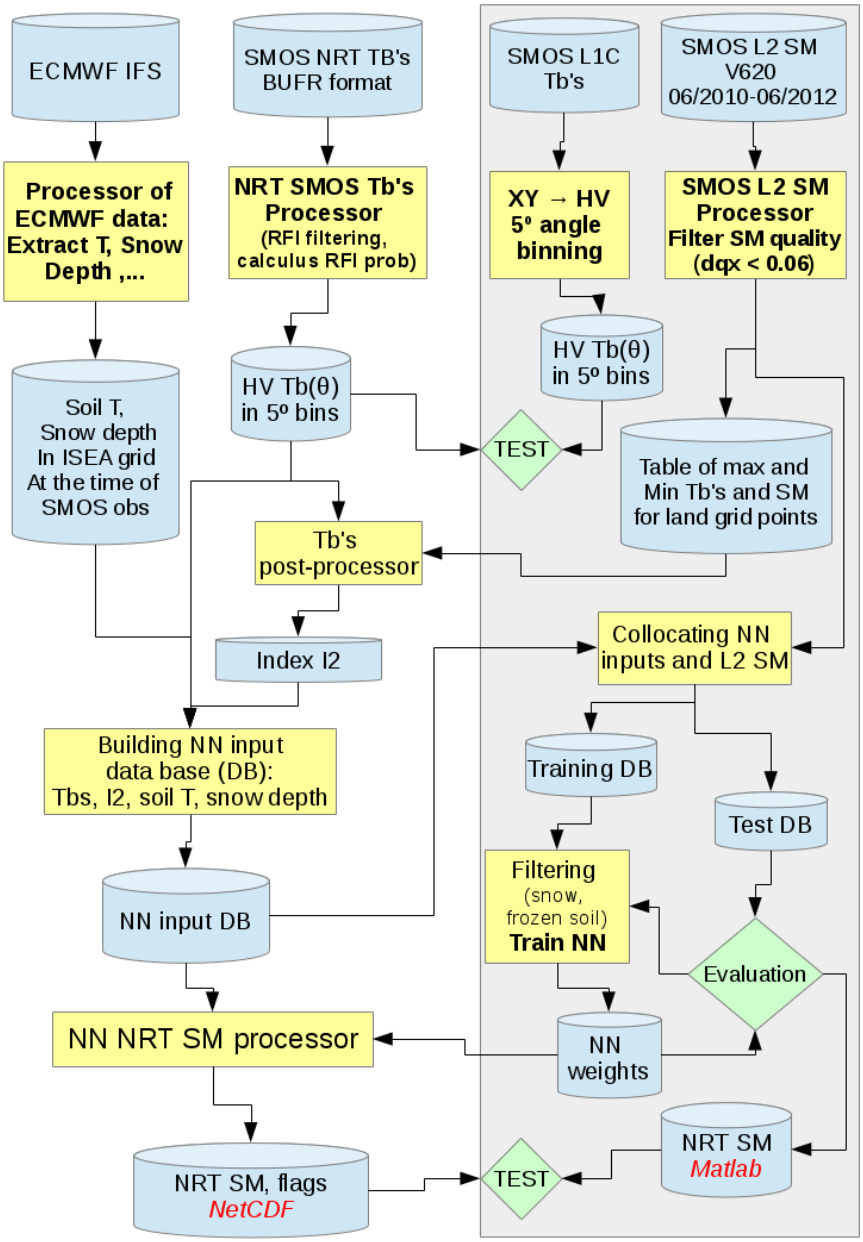

Figure 8: Flow chart of the NRT SM processor. The right-hand part, shown in a grey box, is the off-line processor (see Sect. 5).

The inputs range should be re-normalized to have values in the $[-1, 1]$ range. If for each input vector element, the minimum and maximum values found during the training phase are given by the vectors v_i^{min} and v_i^{max} $(i = 1, ..., n_{in})$, the normalization can be computed as follows:

$$v_i^{norm} = -1 + 2\frac{v_i - v_i^{min}}{v_i^{max} - v_i^{min}},\ \forall i = 1...n_{in} \tag{3}$$

The normalized input, together with the first layer weights (W_{L1}) and bias B_{L1} are used to compute the first layer outputs v^{L1} as follows:

$$v_j^{L1} = \tanh(\sum_{i=1}^{n_{in}} W_{L1}^{ij}\, v_i^{norm} + B_{L1}^j),\ \forall j = 1...n_{L1} \tag{4}$$

The output of the second layer is computed from the first layer outputs, and the second layer weights (W_{L2}) and bias B_{L2} as follows:

$$v^{L2} = \sum_{j=1}^{n_{L1}} W_{L2}^j v_j^{L1} + B_{L2} \tag{5}$$

The values of the weights W_{L1} and W_{L2} and the bias B_{L1} and B_{L2} are determined after the training phase. The exact values for the operational NRT SM processor can be found in Muñoz-Sabater et al. (2016). Finally, to obtain the NN output (v^{out}), the output of the second layer has to be re-normalized as follows:

$$v^{out} = v_{newMin}^{L2} + \frac{v_{newMax}^{L2} - v_{newMin}^{L2}}{v_{oldMax}^{L2} - v_{oldMin}^{L2}}(v^{L2} - v_{oldMin}^{L2}); \tag{6}$$

5.2.1 Neural network output uncertainties

From the definitions of $I_{2_{\lambda\phi}}(t)$ and $I_{1_{\lambda\phi}}(t)$ given by Eqs. 1 and 2, their associated uncertainties $\Delta I_{2_{\lambda\phi}}(t)$ and $\Delta I_{1_{\lambda\phi}}(t)$ can be computed from uncertainties in $T_{\rm b}$'s, in the maximum and minimum $T_{\rm b}$'s and the associated SM values as follows:

$$\Delta I_{2_{\lambda\phi}}(t) = \left\{[SM_{\lambda\phi}^{T_b^{max}} - SM_{\lambda\phi}^{T_b^{min}}]^2(\Delta I_{1_{\lambda\phi}}(t))^2 + [1 - I_{1_{\lambda\phi}}(t)]^2(\Delta SM_{\lambda\phi}^{T_b^{min}})^2 + [I_{1_{\lambda\phi}}(t)]^2(\Delta SM_{\lambda\phi}^{T_b^{max}})^2\right\}^{1/2} \tag{7}$$

Where $\Delta I_{1_{\lambda\phi}}(t)$ is given by:

$$\Delta I_{1_{\lambda\phi}}(t) = \frac{1}{T_{D_{\lambda\phi}}}\left[\Delta T_{b_{\lambda\phi}}(t)^2 + \left(\frac{T_{m_{\lambda\phi}}(t)}{T_{D_{\lambda\phi}}}\Delta T_{b_{\lambda\phi}}^{max}\right)^2 + \left\{\left(-1 + \frac{T_{m_{\lambda\phi}}(t)}{T_{D_{\lambda\phi}}}\right)\Delta T_{b_{\lambda\phi}}^{min}\right\}^2\right]^{1/2}, \tag{8}$$

(9)

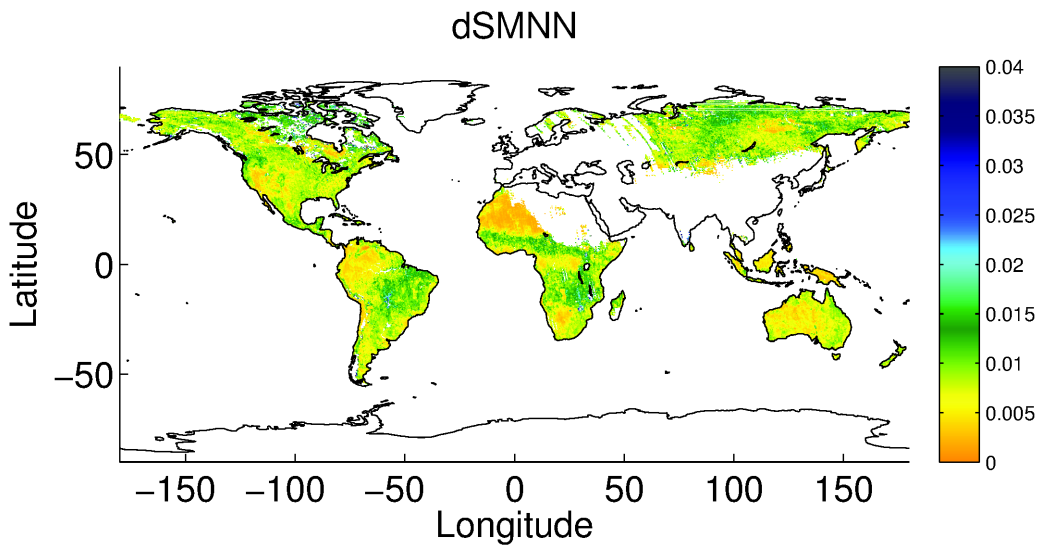

Figure 9: Example of the neural network output uncertainty taking into account the uncertainty in the inputs as described in Sect. 5.2.1. The figure shows the monthly mean for september 2012 of the output uncertainties of a neural network using as input Tb's from 7 angles bins 25 to 60° for H and V polarizations and the associated indexes I_2. In this example the reference SM used to train the NN were ECMWF simulated fields for which the associated uncertainty used to compute ΔI_2 is supposed to be 0.01 m^3/m^3.

as a function of the uncertainty of the local instantaneous measurement $\Delta T_{b_{\lambda\phi}}(t)$ and the uncertainties of the local extreme T_b's values ($\Delta T_{b_{\lambda\phi}}^{max}$ and $\Delta T_{b_{\lambda\phi}}^{min}$).

The uncertainties of the NN output given by Eqs. 3-6 can be estimated from the uncertainties in the input vector elements (Δv_i) as follows. First the uncertainties of the normalized input vector can be computed as:

$$\Delta v_i^{norm} = 2\frac{\Delta v_i}{v_i^{max} - v_i^{min}},\ \forall i = 1...n_{in} \tag{10}$$

Using those quantities, the uncertainty of the two layers neural network given by Eqs. 4 and 5 can be expressed as:

$$(\Delta v^{L2})^2 = \sum_{i=1}^{n_{in}} \left\{ (\Delta v_i^{norm})^2 \left(\sum_{j=1}^{n_{L1}} W_{L2}^j W_{L1}^{ij} \sigma^j \right)^2 \right\} \tag{11}$$

where σ^j is given by:

$$\sigma^j = 1 - \tanh^2(\sum_{i=1}^{n_{in}} W_{L1}^{ij}\, v_i^{norm} + B_{L1}^j),\ \forall j = 1...n_{L1} \tag{12}$$

Finally, the uncertainty after the normalization of the output can be written as:

$$\Delta v^{out} = \frac{v^{L2}_{newMax} - v^{L2}_{newMin}}{v^{L2}_{oldMax} - v^{L2}_{oldMin}} \Delta v^{L2}; \tag{13}$$

Expressing the output uncertainty as Eq. 11 implies that the vector elements v_i are independent. However, when using index I_2 as input as well as the actual $T_{\rm b}$'s, some elements are not independent. Since the uncertainties in Eq. 11 are expressed in quadratic form, Eq. 11 gives an upper limit to the output uncertainty. Figure 9 show an example of the output uncertainty for a NN using $T_{\rm b}$'s and local indexes I_2 as inputs.

6 Summary

The best approach to retrieve soil moisture in Near-Real-Time (NRT) using networks has been discussed using SMOS CATDS Level 3 brightness temperatures and Level 3 soil moisture (SM). Neural network retrievals have been first evaluated comparing the output SM to the L3 SM used as reference during 2012. The global daily correlation ("spatial correlation") and the local temporal correlations have also been computed and averaged in the June-2010 to June 2013 period. The NNs output has also been evaluated against in situ measurements over the SCAN network, the USDA ARS watersheds and OzNet.

The recommended input configuration is using SMOS $T_{\rm b}$'s from 30° to 45 ° incidence angles in 5° bins for both H and V polarizations, the corresponding I_2 normalized indexes, and the 0-7 cm soil temperature forecast by ECMWF. The recommended NN architecture is two layers with a hidden layer containing 5 non-linear neurons and an output layer with one linear neuron. This configuration is the best trade-off of retrieved SM performance and retrieval swath width (914 km).

The recommended NN configuration for the NRT SM product has been specifically evaluated against the reference L3 SM data and against a large number of in situ measurements from the International Soil Moisture Network. Average statistics are somewhat better than those of the reference L3 SM data for most of the sites.

In summary, the recommended NN configuration performs as well or better than the reference SM dataset but the retrieval can be done in Near-Real-Time after a global training phase. Finally, the proposed global architecture of the NRT SM processor has been discussed and the NN algorithm has been described including the output uncertainty estimation.

References

Berthon, L., et al., 2013: CATDS Level 3 data product description: Soil Moisture and Brightness Temperature part. *CESBIO report SO-TN-CB-CA-0001*, 1–38.

de Rosnay, P., M. Dragosavac, M. Drusch, A. Gutiérrez, M. Rodríguez López, N. Wright, J. Muñoz Sabater, and C. R., 2012: SMOS NRT BUFR specification. SMOS-NRT-BUFR-ECMWF - v2.0, ECMWF.

Dorigo, W., et al., 2011: The international soil moisture network: a data hosting facility for global in situ soil moisture measurements. *Hydrology and Earth System Sciences*, 15 (5), 1675–1698.

Jackson, T. J., et al., 2012: Validation of soil moisture and ocean salinity (SMOS) soil moisture over watershed networks in the US. *Geoscience and Remote Sensing, IEEE Transactions on*, 50 (5), 1530–1543.

Kerr, Y. H., et al., 2016: Overview of smos performance in terms of global soil moisture monitoring after six years in operation. *Remote Sensing of Environment*, 180, 40–63.

Mecklenburg, S., et al., 2016: Esa's soil moisture and ocean salinity mission: From science to operational applications. *Remote Sensing of Environment*, 180, 3–18.

Muñoz-Sabater, J., N. J. Rodríguez-Fernández, P. Richaume, P. de Rosnay, and Y. H. Kerr, 2016: SMOS Near-Real-Time Soil Moisture processor. Tech. Rep. ECMWF ESA report, ECMWF, Reading, UK.

Quesney, A., 2011: Data Processing Model: traitements L3TB. Tech. Rep. CAT-DPM-CTL3TB-00061-CG, CapGemini Sud / ACRI-ST.

Rodríguez-Fernández, N. J., J. Muñoz-Sabater, P. Richaume, C. Albergel, P. de Rosnay, and Y. H. Kerr, 2016: Evaluation of the SMOS Near-Real-Time soil moisture. *in prep.*

Rodríguez-Fernández, N. J., P. Richaume, F. Aires, C. Prigent, J. Kerr, Y. H. Kolassa, C. Jiménez, F. Cabot, and A. Mahmoodi, 2013: Soil moisture retrieval from SMOS observations using neural networks. Tech. Rep. SMOS Ground Segment SO-TN-CB-GS-038, CESBIO, Toulouse, France.

Rodríguez-Fernández, N. J., P. Richaume, Y. H. Kerr, F. Aires, C. Prigent, C. Jiménez, and A. Mahmoodi, 2014: Retrieving soil moisture from SMOS brightness temperatures by neural networks trained with simulated data. Tech. Rep. SMOS Ground Segment SO-TN-CB-GS-041, CESBIO, Toulouse, France.

Rodríguez-Fernández, N. J., et al., 2015: Soil moisture retrieval using neural networks: application to SMOS. *IEEE Transactions on Geoscience and Remote Sensing*, Volume:53 , Issue: 11, 5991–6007.

Schaefer, G., M. Cosh, and T. Jackson, 2007: The USDA natural resources conservation service soil climate analysis network (SCAN). *Journal of Atmospheric and Oceanic Technology*, 24 (12), 2073–2077.

Smith, A. B., et al., 2012: The murrumbidgee soil moisture monitoring network data set. *Water Resour. Res.*, 48.